4728 *Chem. Mater.* **2010,** *22,* 4728–4739
DOI:10.1021/cm101036a

CHEMISTRY OF MATERIALS
Article

Polymer-Stabilized Lanthanide Fluoride Nanoparticle Aggregates as Contrast Agents for Magnetic Resonance Imaging and Computed Tomography

Evelyn Ning Man Cheung,[‡] Rohan D. A. Alvares,[†] Wendy Oakden,[§] Richa Chaudhary,[†] Melissa L. Hill,[§] Jothirmayanantham Pichaandi,[⊥] Gary C. H. Mo,[∥] Christopher Yip,[‡] Peter M. Macdonald,[†] Greg J. Stanisz,[§] Frank C. J. M. van Veggel,[⊥] and R. Scott Prosser*[,†,‡]

[‡]*Department of Biochemistry, University of Toronto, 1 King's College Circle, Medical Sciences Building, Room 5207, Toronto, ON, Canada, M5S 1A8,* [†]*Department of Chemistry, University of Toronto, UTM, 3359 Mississauga Rd. North, Mississauga, ON, Canada, L5L 1C6,* [§]*Sunnybrook Health Sciences Centre 2075 Bayview Avenue, S-Wing, Suite S672 Toronto, ON, Canada and Department of Medical Biophysics, University of Toronto, Toronto, ON, Canada, M5G 2M9,* [⊥]*Department of Chemistry, University of Victoria Victoria, BC, Canada, V8W 3 V6, and* [∥]*Chemical Engineering and Applied Chemistry, University of Toronto, Toronto, ON, Canada, M5G 2M9*

Received April 14, 2010. Revised Manuscript Received June 30, 2010

Poly(acrylic acid) consisting of 25 monomer units (PAA_{25}) was used to stabilize nanoparticle aggregates (NPAs) consisting of either $NaGdF_4$ or 50/50 mixtures of GdF_3 and CeF_3. The resulting polymer-stabilized nanoparticle aggregates (NPAs) were developed and tested for their application as contrast agents for magnetic resonance imaging (MRI) and computed tomography (CT). The PAA_{25}-stabilized NPAs exhibit low polydispersity and are colloidally stable at concentrations of 40 mg/mL, while their sizes can be be controlled by choosing a specific ratio of Gd^{3+} to Ce^{3+}. Scanning transmission electron microscopy (STEM) reveals that $NaGdF_4$ NPAs possess an average diameter of 400 nm. High-resolution STEM and powder X-ray diffraction (XRD) both show that these NPAs consist of a stable aggregate of smaller NPs, whose diameters are 20−22 nm. PAA_{25}-stabilized NPAs consisting of a 50/50 mixture of GdF_3 and CeF_3 possess an average diameter of 70 nm, while the fundamental unit size is estimated to be 10−12 nm in diameter. The PAA_{25}-stabilized GdF_3/CeF_3 NPAs possess mass relaxivities of 40 ± 2 and 30 ± 2 s^{-1} $(mg/mL)^{-1}$ at 1.5 T and 3.0 T, respectively. Their effectiveness as contrast agents for CT X-ray imaging at various X-ray energies was also tested and compared to that of equivalent mass concentrations of Gd^{3+}-diethylene triamine pentaacetic acid (Gd^{3+}-DTPA) and iopromide. Gd-based NPAs exhibit superior CT contrast to equal-mass concentrations of either iopromide or Gd^{3+}-DTPA below 30 keV and above 50 keV. Finally, PAA_{25} was functionalized by folic acid to explore targeted imaging. Confocal microscopy revealed that, by functionalizing the PAA_{25}-stabilized $NaGdF_4$:Tb^{3+} NPAs with ∼0.8 folates per polymer, binding and endocytosis occurred in SK-BR-3 human breast cancer cells. The utility of the PAA_{25}-stabilized GdF_3/CeF_3 NPAs for MRI is demonstrated in rat perfusion MRI experiments, where T_1-weighted MRI images of equivalent concentrations of either Gd^{3+}-DTPA or the above NPAs are directly compared. The high relaxivities provide an opportunity to conduct perfusion MRI experiments with significantly lower concentrations than those needed for current commercial agents.

Introduction

Thirty to forty percent of magnetic resonance imaging (MRI) and computed tomography (CT) clinical applications use injected tracers to improve contrast.[1−8] In MRI, such diagnostics consist of paramagnetic complexes such as iron oxides[9] or chelates of gadolinium (Gd^{3+}).[10,11] Gd^{3+} is one of the most effective paramagnetic contrast agents, because of its high number of unpaired electrons and its relatively long electronic spin relaxation time, which serves to decrease spin−lattice and spin−spin relaxation times (i.e., T_1, T_2, and T_2^*) of ^1H nuclei in its vicinity.[12]

*Author to whom correspondence should be addressed. E-mail: scott.prosser@utoronto.ca.

(1) Elke, M. *Experientia* **1995**, *51*, 665–680.
(2) Weinmann, H. J.; Ebert, W.; Misselwitz, B.; Schmitt-Willich, H. *Eur. J. Radiol.* **2003**, *46*, 33–44.
(3) Wu, E. X.; Tang, H. Y.; Jensen, J. H. *NMR Biomed.* **2004**, *17*, 478–483.
(4) Querol, M.; Bogdanov, A. *J. Magn. Reson. Imaging* **2006**, *24*, 971–982.
(5) Lin, S. P.; Brown, J. J. *J. Magn. Reson. Imaging* **2007**, *25*, 884–899.
(6) Caravan, P. *Chem. Soc. Rev.* **2006**, *35*, 512–523.
(7) Barrett, T.; Kobayashi, H.; Brechbiel, M.; Choyke, P. L. *Eur. J. Radiol.* **2006**, *60*, 353–366.
(8) Frullano, L.; Meade, T. J. *J. Biol. Inorg. Chem.* **2007**, *12*, 939–949.
(9) Bulte, J. W. M.; Kraitchman, D. L. *NMR Biomed.* **2004**, *17*, 484–499.
(10) Aime, S.; Botta, M.; Terreno, E. *Adv. Inorg. Chem.* **2005**, *57*, 173–237.
(11) Zhang, K. *Biomaterials* **2004**, *25*, 5281–5291.
(12) Toth, E.; Helm, L.; Merbach, A. E. *Top. Curr. Chem.* **2002**, *221*, 61–101.

Published on Web 07/23/2010

The effectiveness of Gd^{3+} as a contrast agent for MRI and CT can be improved significantly by bundling many ions together in the form of an appropriately stabilized complex or nanoparticle. In this paper, we focus on the application of polymer-stabilized lanthanide fluoride nanoparticle aggregates (i.e., $NaLnF_4$ and LnF_3 nanoparticle aggregates (NPAs)) for contrast enhancement in T_1-weighted MRI. The sizes of the LnF_3 NPAs (70 nm) are ideal for vascular retention and tumor penetration, while the MRI contrast is 5−7 times higher than that observed with equivalent mass concentrations of Gd^{3+} chelates used in current clinical applications.

An MRI contrast agent may be evaluated through its "relaxivity", which refers to the paramagnetic component of spin−lattice or spin−spin relaxation rates ($1/T_1$ or $1/T_2$) per unit concentration of contrast agent. Using T_1- or T_2-weighted imaging, clinicians can better distinguish a region of interest of abnormal pathology, providing it contains an excess of contrast agent.[13−19] Because of its limited solubility and high toxicity, Gd^{3+} is administered as a chelate, which prevents leaching of the ion into the body. The way in which water coordinates with the chelate (i.e., geometry, strength of ionic interactions, coordination number) and its exchange lifetime with bulk solvent greatly affect the observed relaxivity. For this reason, a great deal of research has focused on chelate design for purposes of optimizing relaxivity under different physiological conditions.[12] High relaxivities are advantageous in targeted imaging or perfusion imaging to increase sensitivity in regions of tissue where the concentration of the contrast agent is low.[20] Relaxivities can be improved by combining many Gd^{3+} ions in the form of micelles,[21] polyamino acids,[22] polysaccharides,[23] dendrimers,[24,25] zeolites,[26] metallofullerenes,[27] or nanoparticles (NPs).[28−37]

The advent of quantum dots as an alternative to organic dyes and fluorescent proteins has revolutionized optical imaging through improved contrast (brightness), reduced photobleaching, and multiplexing technology.[38] Nanoparticles may offer similar gains over small molecules in the MRI field, in terms of dramatic improvements in contrast, improved cell specificity, and vascular retention. We present a class of LnF_3 nanoparticle aggregates comprised of a mixture of GdF_3 and CeF_3 and coated with linear poly(acrylic acid) chains consisting of 25 repeating units (PAA_{25}). These aggregates, whose sizes depend on the ratio of Gd^{3+} to Ce^{3+}, are shown to have a fine structure consisting of smaller nanoparticles. The high surface area associated with the NPAs is ideal for maximizing contact with water molecules and, hence, optimizing contrast in MRI.

Size and morphology are also known to influence stability, biodistribution, opsonization, metabolism, toxicity, and clearance.[39,40] Prior work with clinical doses of intravenously delivered iron oxide NPs revealed that these NPs are generally cleared via macrophages in the liver, spleen, and bone marrow, with half-lives ranging from less than an hour to days, depending on size and coating agent. The surface properties also dictate colloidal stability, which may change substantially upon delivery. Typically, the aggregate size must exceed 20−30 nm to avoid renal excretion, while vascular fenestrations facilitate the leakage of nanoparticles across endothelial barriers. These fenestrations are highly dependent on tissue type and may range from 20−30 nm in the kidney to 150 nm or more in the liver, spleen, and lung. It has been suggested that nanoparticle aggregate sizes of 70−200 nm are ideal for deposition into tumors via such fenestrations, while a size of 50 nm achieves penetration of NPs through extracellular spaces in live tumors. The 50/50 CeF_3/GdF_3 NPAs discussed below possess an

(13) Filippi, M.; Grossman, R. I. *Neurology* **2002**, *58*, 1147–1153.
(14) Zivadinov, R.; Bakshi, R. *Front. Biosci.* **2004**, *9*, 665–683.
(15) Kim, Y. H. *Ind. Health* **2004**, *42*, 111–115.
(16) Symms, M.; Jager, H. R.; Schmierer, K.; Yousry, T. A. *J. Neurol. Neurosurg. Psychiatry* **2004**, *75*, 1235–1244.
(17) Lanza, G. M.; Winter, P. M.; Neubauer, A. M.; Caruthers, S. D.; Hockett, F. D.; Wickline, S. A. *Curr. Top. Dev. Biol.* **2005**, *70*, 57–76.
(18) Bakshi, R. *J. Neuroimag.* **2005**, *15*, 5S–9S.
(19) Atmaca, M.; Yildirim, H.; Ozdemir, H.; Tezcan, E.; Poyraz, A. K. *Progress Neuro-Psychopharmacol. Biol. Psychiatry* **2007**, *31*, 46–52.
(20) Livramento, J. B.; Toth, E.; Sour, A.; Borel, A.; Merbach, A. E.; Ruloff, R. *Angew. Chem., Int. Ed.* **2005**, *44*, 1480–1484.
(21) Andre, J. P.; Toth, E.; Fischer, H.; Seelig, A.; Macke, H. R.; Merbach, A. E. *Chem—Eur. J.* **1999**, *5*, 2977–2983.
(22) Aime, S.; Botta, M.; Garino, E.; Crich, S. G.; Giovenzana, G.; Pagliarin, R.; Palmisano, G.; Sisti, M. *Chem—Eur. J.* **2000**, *6*, 2609–2617.
(23) Lu, Z. R.; Parker, D. L.; Goodrich, K. C.; Wang, X. H.; Dalle, J. G.; Buswell, H. R. *Magn. Reson. Med.* **2004**, *51*, 27–34.
(24) Wiener, E. C.; Brechbiel, M. W.; Brothers, H.; Magin, R. L.; Gansow, O. A.; Tomalia, D. A.; Lauterbur, P. C. *Magn. Reson. Med.* **1994**, *31*, 1–8.
(25) Yan, G. P.; Bottle, S. E.; Zhuo, R. X.; Wei, L.; Liu, M. L.; Li, L. Y. *J. Bioact. Compat. Polym.* **2004**, *19*, 453–465.
(26) Platas-Iglesias, C.; Vander Elst, L.; Zhou, W. Z.; Muller, R. N.; Geraldes, C.; Maschmeyer, T.; Peters, J. A. *Chem—Eur. J.* **2002**, *8*, 5121–5131.
(27) Sitharaman, B.; Bolskar, R. D.; Rusakova, I.; Wilson, L. J. *Nano Lett.* **2004**, *4*, 2373–2378.
(28) Singh, R.; Kostarelos, K. *Trends Biotechnol.* **2009**, *27*, 220–229.
(29) Paunesku, T.; Ke, T.; Dharmakumar, R.; Mascheri, N.; Wu, A. G.; Lai, B.; Vogt, S.; Maser, J.; Thurn, K.; Szolc-Kowalska, B.; Larson, A.; Bergan, R. C.; Omary, R.; Li, D. B.; Lu, Z. R.; Woloschak, G. E. *Nanomed.−Nanotechnol. Biol. Med.* **2008**, *4*, 201–207.
(30) Werner, E. J.; Datta, A.; Jocher, C. J.; Raymond, K. N. *Angew. Chem., Int. Ed.* **2008**, *47*, 8568–8580.
(31) Uchida, M.; Terashima, M.; Cunningham, C. H.; Suzuki, Y.; Willits, D. A.; Willis, A. F.; Yang, P. C.; Tsao, P. S.; McConnell, M. V.; Young, M. J.; Douglas, T. *Magn. Reson. Med.* **2008**, *60*, 1073–1081.
(32) Cormode, D. P.; Skajaa, T.; Fayad, Z. A.; Mulder, W. J. M. *Arterioscler. Thromb. Vasc. Biol.* **2009**, *29*, 992–1000.
(33) Carniato, F.; Tei, L.; Dastru, W.; Marchese, L.; Botta, M. *Chem. Commun.* **2009**, 1246–1248.
(34) Datta, A.; Hooker, J. M.; Botta, M.; Francis, M. B.; Aime, S.; Raymond, K. N. *J. Am. Chem. Soc.* **2008**, *130*, 2546–2552.
(35) Liepold, L.; Anderson, S.; Willits, D.; Oltrogge, L.; Frank, J. A.; Douglas, T.; Young, M. *Magn. Reson. Med.* **2007**, *58*, 871–879.
(36) Bridot, J. L.; Faure, A. C.; Laurent, S.; Rivière, C.; Billotey, C.; Hiba, B.; Janier, M.; Josserand, V.; Coll, J. L.; Elst, L. V.; Muller, R.; Roux, S.; Perriat, P.; Tillement, O. *J. Am. Chem. Soc.* **2007**, *129*, 5076–84.
(37) Hartman, K. B.; Laus, S.; Bolskar, R. D.; Muthupillai, R.; Helm, L.; Toth, E.; Merbach, A. E.; Wilson, L. J. *Nano Lett.* **2008**, *8*, 415–419.
(38) Walling, M. A.; Novak, J. A.; Shepard, J. R. E. *Int. J. Mol. Sci.* **2009**, *10*, 441–491.
(39) Corot, C.; Robert, P.; Idée, J.-M.; Port, M. *Adv. Drug Delivery Rev.* **2006**, *58*, 1471–504.
(40) Moghimi, S. M.; Hunter, A. C.; Murray, J. C. Pharmacol. Rev. **2001**, *53* (2), 283−318.

average diameter of 70 nm, which suggests ideal retention profiles and improved passive targeting.

Certain tumor cells are known to overexpress membrane folate receptors, resulting in a high uptake of folate-tagged moieties. By tagging PAA_{25}-stabilized NPAs with folic acid (FA) via a short linker, the NPAs then actively target cancer cells such as the SK-BR-3 breast cancer cells, as shown by confocal fluorescence microscopy. We demonstrate their application and discuss their potential use in MRI and CT imaging of tumors. Furthermore, we show that our synthetic approach can easily be optimized to achieve high cell specificity. We begin by discussing general features of MRI contrast agents, including properties that must be considered when implementing nanoparticle aggregates for this purpose. We then discuss the synthetic protocol and characterization of the nanoparticle aggregates, followed by confocal microscopy imaging studies of folic acid-ligated NPAs, and both CT and MRI results of phantom samples and live animals.

Nanoparticle Design Concepts for Optimizing Water Spin Relaxation. The relaxation of water proton spins in the vicinity of a paramagnetic species such as Gd^{3+} originates from the dipole−dipole interactions between the proton nuclear spins and the fluctuating local magnetic field caused by the unpaired electron spins of Gd^{3+}.[41,42] The electronic spin relaxation times (T_{1e} and T_{2e}), the exchange rate of water between the inner sphere and the bulk state (k_{ex}), and the tumbling time of the Gd^{3+}:chelate complex directly influence this fluctuating field and the observed paramagnetic rate.[12] Relaxation arises primarily from inner-sphere water molecules (i.e., those in the first coordination sphere of Gd^{3+}), which, in turn, give rise to a bulk effect through chemical exchange of water molecules. Thus, the paramagnet concentration, the number of water molecules per Gd^{3+} species, and the average residence time of water in the first hydration shell, τ_m (which is defined as $\tau_m = 1/k_{ex}$), are additional parameters that influence the relaxation rate.[12] Finally, the paramagnetic relaxation rate, arising from the inner-shell interaction, is acutely sensitive to the Gd^{3+}-proton distance and geometry of the Gd^{3+}:H_2O complex, which, in turn, dictates the value of T_1 associated with bound water (T_{1m}). Ideally, T_{1m} should be very short, and the residence time (τ_m) should be much less than the tumbling time (τ_R).

A considerable body of literature exists on materials designed with the above parameters in mind.[30] The strategy is to bring together a large number of Gd^{3+} ions in such a way as to significantly increase the tumbling time, τ_R, of the complex, while leaving as many inner-shell waters in contact with the nanoparticle surface as possible. Nanoparticle surface charge, and polymer coatings are also expected to strongly influence the effective water exchange rate, k_{ex}, and, thus, the observed water T_1 value. Furthermore, core Gd^{3+} ions, which are effectively inaccessible to surface waters in larger nanoparticles, will be expected to contribute little to the overall relaxivity. Therefore, the challenge is to synthesize the nanoparticle aggregates with the highest possible porosity or access to water, while of sufficient diameter to achieve a long tumbling time τ_R and, consequently, a high relaxivity. In this scenario, the water residence time may also be relatively short, since its coordination with a given Gd^{3+} ion on the surface of the nanoparticle may be sterically perturbed by the polymer coating.

The application of inorganic nanoparticles as MRI contrast agents has focused primarily on iron oxide superparamagnetic nanoparticles or Gd^{3+}-based nanoparticles. The iron oxides give paramagnetic effects that are confined largely to T_2 or T_2^* relaxation and are thus used primarily for negative contrast imaging.[43−49] More recently, inorganic and water-soluble nanoparticle complexes based on Gd^{3+} formulations have achieved superior positive contrast via T_1-weighted imaging. These include GdF_3,[50] Gd_2O_3,[36,51−56] $GdPO_4$,[57] $Gd(OH)_3$,[58] mesoporous silica-coated GdF_3 nanoparticles,[59,60] and organic−inorganic hybrid frameworks.[61] In some cases, molar relaxivities, on a per Gd^{3+} basis, have been shown to be 2−3 times better than current commercial Gd^{3+} chelates (Gd^{3+}-DTPA). Generally, the nanoparticle coatings are designed to improve the dispersibility and allow functionalization for the purpose of regulating clearance or enabling the covalent attachment of targeting agents.

The current work builds upon an earlier paper,[50] in which citrate and 2-aminoethyl phosphate-stabilized

(41) Bloembergen, N.; Purcell, E. M.; Pound, R. V. *Phys. Rev.* **1948**, *73*, 679–712.
(42) Aime, S.; Botta, M.; Terreno, E. Adv. Inorg. Chem. **2005**, *57*, 173−237.
(43) Xie, J.; Huang, J.; Li, X.; Sun, S.; Chen, X. *Curr. Med. Chem.* **2009**, *16*, 1278–1294.
(44) Wu, W.; He, Q. G.; Jiang, C. Z. *Nanoscale Res. Lett.* **2008**, *3*, 397–415.
(45) Laurent, S.; Forge, D.; Port, M.; Roch, A.; Robic, C.; Elst, L. V.; Muller, R. N. *Chem. Rev.* **2008**, *108*, 2064–2110.
(46) Thorek, D. L. J.; Chen, A.; Czupryna, J.; Tsourkas, A. *Ann. Biomed. Eng.* **2006**, *34*, 23–38.
(47) Teja, A. S.; Koh, P. Y. *Prog. Cryst. Growth Charact. Mater.* **2009**, *55*, 22–45.
(48) Peng, X. H.; Qian, X. M.; Mao, H.; Wang, A. Y.; Chen, Z.; Nie, S. M.; Shin, D. M. *Int. J. Nanomed.* **2008**, *3*, 311–321.
(49) Na, H. B.; Song, I. C.; Hyeon, T. *Adv. Mater.* **2009**, *21*, 2133–2148.
(50) Evanics, F.; Diamente, P. R.; van Veggel, F. C. J. M.; Stanisz, G. J.; Prosser, R. S. *Chem. Mater.* **2006**, *18*, 2499–2505.
(51) Bridot, J. L.; Dayde, D.; Riviere, C.; Mandon, C.; Billotey, C.; Lerondel, S.; Sabattier, R.; Cartron, G.; Le Pape, A.; Blondiaux, G.; Janier, M.; Perriat, P.; Roux, S.; Tillement, O. *J. Mater. Chem.* **2009**, *19*, 2328–2335.
(52) McDonald, M. A.; Watkin, K. L. *Investig. Radiol.* **2003**, *38*, 305–10.
(53) McDonald, M. A.; Watkin, K. L. *Acad. Radiol.* **2006**, *13*, 421–427.
(54) Park, J. Y.; Choi, E. S.; Baek, M. J.; Lee, G. H.; Woo, S.; Chang, Y. *Eur. J. Inorg. Chem.* **2009**, 2477–2481.
(55) Park, J. Y.; Baek, M. J.; Choi, E. S.; Woo, S.; Kim, J. H.; Kim, T. J.; Jung, J. C.; Chae, K. S.; Chang, Y; Lee, G. H. *ACS Nano* **2009**, *3*, 3663–3669.
(56) Petoral, R. M.; Soderlind, F.; Klasson, A.; Suska, A.; Fortin, M. A.; Abrikossova, N.; Selegard, L.; Kall, P. O.; Engstrom, M.; Uvdal, K. *J. Phys. Chem. C* **2009**, *113*, 6913–6920.
(57) Hifumi, H.; Yamaoka, S.; Tanimoto, A.; Citterio, D.; Suzuki, K. *J. Am. Chem. Soc.* **2006**, *128*, 15090–15091.
(58) Lee, B. I.; Lee, K. S.; Lee, J. H.; Lee, I. S.; Byeon, S. H. *Dalton Trans.* **2009**, 2490–2495.
(59) Rieter, W. J.; Kim, J. S.; Taylor, K. M. L.; An, H. Y.; Lin, W. L.; Tarrant, T.; Lin, W. B. *Angew. Chem., Int. Ed.* **2007**, *46*, 3680–3682.
(60) Taylor, K. M. L.; Kim, J. S.; Rieter, W. J.; An, H.; Lin, W. L.; Lin, W. B. *J. Am. Chem. Soc.* **2008**, *130*, 2154–2155.
(61) Rowe, M. D.; Thamm, D. H.; Kraft, S. L.; Boyes, S. G. *Biomacromolecules* **2009**, *10*, 983–993.

GdF_3 nanocrystals were synthesized and evaluated for their potential as MRI contrast agents. Herein, we explore the use of an alternative stabilizing agent (poly(acrylic acid)) and a modified two-step synthetic protocol, which is intended to improve size control and generate monodisperse nanoparticle aggregates with higher relaxivities.

Materials and Methods

Sodium fluoride (99%), *N,N′*-dicyclohexylcarbodiimide, 1-ethyl-3-(3-dimethylaminopropyl)carbodiimide, *N*-hydroxysuccinimide, $Ce(NO_3)_3 \cdot 6H_2O$ (99.9%), $Tb(NO_3)_3 \cdot 6H_2O$ (99.9%), $Y(NO_3)_3 \cdot 6H_2O$ (99.9%), $Eu(NO_3)_3 \cdot 6H_2O$ (99.9%), $Gd(NO_3)_3 \cdot 6H_2O$ (99.9%), and poly(acrylic acid) (PAA, MW = 1800 g/mol) were purchased from Sigma−Aldrich (Mississauga, ON, Canada). Citric acid (99.5%) and aqueous ammonium hydroxide (28−30%) were purchased from EMD Chemicals, Inc. (Gibbstown, NJ).

Citrate-Coated Lanthanide Fluoride Nanoparticle Aggregate Synthesis. While alternative synthetic methods are possible,[62] citrate-coated lanthanide fluoride nanoparticle aggregates (NPAs) were produced via a coprecipitation method, using a slight modification of our earlier protocol.[50] A solution containing citric acid (0.41 g, 2.13 mmol) and sodium fluoride (0.043 g, 1.00 mmol) in distilled water (25 mL) was neutralized using 12 M ammonium hydroxide. The solution was then heated in a round-bottomed flask to a temperature of 75 ± 5 °C using an oil bath. Typically, a stir rate of 500−750 rpm was used. Higher stir rates generally resulted in smaller aggregate size. An aqueous lanthanide nitrate solution (0.44 mmol of $Ln(NO_3)_3$ in 2 mL of distilled water) was titrated into the round-bottomed flask at a rate of 2 mL/h, using a syringe pump (New Era Pump Systems, NE-1000) fitted with a 26G1/2 needle, yielding a translucent solution. If multiple lanthanides were used, the lanthanide nitrates [$Gd(NO_3)_3$, $Ce(NO_3)_3$, and/or $Tb(NO_3)_3$, $Eu(NO_3)_3$] were first combined before being added dropwise. The resulting mixture was left to react for an additional 2 h. The nanoparticles were isolated through precipitation with 50 mL of 95% ethanol, followed by centrifugation at 7000 rpm for 2 min and two rounds of resuspension and washing with acetone. In all, three lanthanide compositions were considered; $NaGdF_4$ and 50/50 CeF_3/GdF_3 NPAs were prepared for purposes of MRI measurements, while 80/20 $NaGdF_4:Tb^{3+}$ NPAs were prepared for epi-fluorescence and confocal microscopy. A 90/10 $NaGdF_4:Eu^{3+}$ lanthanide formulation was used in the CT studies.

PAA_{25}-Stabilized Lanthanide Fluoride Nanoparticle Aggregate Synthesis. Citrate-coated LnF_3 or $NaLnF_4$ NPAs were first synthesized according to the above protocol. A solution consisting of 0.25 mmol of PAA_{25} in 5 mL water was first neutralized using 12 M ammonium hydroxide. This solution was then pipetted into the above 27 mL volume of citrate NPAs. The exchange was allowed to proceed for 12 h at 75 °C. Nanoparticle aggregates were first isolated through precipitation with 50 mL 95% ethanol, followed by two rounds of resuspension and subsequent precipitation with acetone. Note that in studies that involved fluorescence imaging and cancer cell targeting, PAA_{25} was first functionalized with a linker, which was attached to folic acid. To ensure strong binding between PAA_{25} and the (positively charged) nanoparticle aggregate surface, coupling of PAA_{25} to folic acid was limited to 0.8 folates per polymer. Details of the coupling reaction are provided below.

Synthesis of Folate-Conjugated Polyacrylic Acid. Folic acid (0.49 g (1 equiv)) was dissolved in 15 mL of DMSO in a round-bottomed flask while stirring and applying slight heating (just enough to dissolve the added folic acid). A combination of 1.5 molar equivalents of DCC and 1.5 molar equivalents of NHS were then added to the stirring solution, which was then left overnight. The resulting solution was then filtered using a gravity filter. Then, 3 molar equivalents of ethylenediamine were then added to the filtrate, which was left to stir for 3 h. The solution was then precipitated using 100 mL of acetone and collected using a Büchner funnel while washing with ether. At this point, the primary product consisted of folic acid conjugated to ethylenediamine (FA-ED), as evidenced by mass spectrometry (data not shown).

PAA_{25} (0.5 g) was dissolved in 20 mL of 50 mM MES buffer while stirring. A solution of the above synthesized FA-ED was then separately dissolved in 10 mL of MES buffer, whereupon the pH was adjusted to ~7 with ammonium hydroxide. A fresh 5 mL solution containing 10 equiv of EDAC and 10 equiv of NHS in distilled water was then added to the PAA_{25} solution. After 3 min, the FA-ED was added to the solution while stirring. After 10 h, the resulting solution was dialyzed against pH 9 distilled water (adjusted with NaOH solution), yielding the PAA_{25}-ED-FA.

Note that a one-step synthetic protocol was used to make the samples for the CT measurements. This protocol tends to make more aggregated particles over time and has thus been superseded by the above two-step method. Briefly, the lanthanide nitrate solution was dropwise added to a solution of NaF and PAA_{25}, which was stirred for 3−4 h at 85 °C and subsequently precipitated in acetone, resuspended in water filtered, and filtered using a 0.45 μm pore filter (VWR Scientific, USA).

Verification of PAA_{25}:FA Stoichiometry. The absorbance values of known concentrations of PAA_{25}-ED-FA solutions were measured at 355 nm, where folic acid is known to give a prominent absorbance peak (ε = 4965.3 $M^{-1}\,cm^{-1}$).

Elemental Composition by EDS. EDS was done using a Hitachi S-4800 field-emission scanning electron microscopy (FE-SEM) system, which was operated at 20 kV and had a resolution of 129 eV. The dispersion was dried to get a white powder, which was tagged onto the substrate using a double-sided carbon tape and mounted onto the sample holder. Three measurements were done for each sample to calculate averages and standard deviations.

(62) Li, C. X.; Yang, J.; Yang, P. P.; Lian, H. Z.; Lin, J. *Chem. Mater.* **2008**, *20*, 4317–4326.

Determination of Crystalline Structure and Composition of NPs by XRD. XRD patterns were measured with Cr (30 kV, 15 mA) radiation on a Rigaku Miniflex diffractometer using a zero-background holder with variable divergence slit, 4.2° scattering slit, and 0.3 mm receiving slit. The scanning step size was 0.5° 2θ, with a counting time of 2 s per step over the 2θ range of 20−100°. Thirty to forty milligrams (30−40 mg) of sample was ground in an aluminum mortar to form a homogeneous powder. The spectra of the Gd/Ce mixtures closely match those of CeF_3 and seem to be shifted to slightly lower angles, because of the smaller unit cell that resulted from mixing with Gd^{3+}.[63]

Magnetic Resonance Relaxation Measurements. T_1 Measurements of NPA Dispersions at 1.5 and 3.0 T. T_1 measurements at 1.5 and 3 T were performed at room temperature on NPA dispersions in water, using clinical MRI scanners (GE Signa, GE Medical Systems, Milwaukee, WI) and a standard inversion recovery spin echo sequence, with a repetition time (TR) of 2500 ms, an echo time (TE) of 9 ms, and nine inversion recovery times, (TI = 50, 350, 650, 950, 1250, 1550, 1850, 2150, and 2450 ms); the field of view was 12 cm × 6 cm, and the image plane was 128 × 128 with a slice thickness of 5 mm. This allowed for the simultaneous imaging of up to 50 1.5-mL vials. The regions of interest were then drawn for each of the vials at TI = 2450 ms, and the signal, containing an average of 20 voxels for each TI, was then evaluated. The signal-to-noise ratio (SNR) was ∼200. The T_1 relaxation time was evaluated assuming monoexponential T_1 recovery. The average reduced χ^2 of the fitting procedure was 1.2 and did not exceed 1.6. To ensure that the results were reproducible, every relaxivity measurement series was repeated on at least two samples, made from at least two separate synthesis batches.

In Vivo MRI. Imaging was performed with a 3T clinical MRI scanner (GE Signa, GE Medical Systems, Milwaukee, WI) using a surface coil (1 in. × 2 in.). Single slice dynamic contrast-enhanced (DCE) images were acquired using a fast spoiled-gradient spin echo (SPGR) sequence. The field of view (FOV) was 4 cm, the slice thickness was 2 mm, the flip angle was 15°, the number of excitations (NEX) was 20, and the in-plane matrix resolution was 128 × 128. DCE-MRI images were acquired every 20 s over a period of 36 min. A tail vein catheter was used to inject a bolus of 0.4 mL of nanoparticle contrast, at a concentration of 18.6 mg/mL, at the beginning of the DCE scan. The rat (male, 3 months old, Long Evans, Charles River, ON, Canada) was imaged supine with the surface coil placed under the neck. Monitoring was done using a pulsed oximeter, and the animal was anesthetized using isofluorane gas at 2% concentration.

X-ray Imaging of NP Dilutions. Samples of PAA_{25}-coated 90/10 $NaGdF_4$:Eu^{3+} NPAs, Gd^{3+}-DTPA, and IP (iopromide) were diluted in water to particle mass concentrations of 20, 30, 40, and 50 mg/mL. The dilutions and a water control were sealed in Eppendorf tubes and placed flat, in order of increasing concentration, directly on the detector cover of a Senographe 2000D digital mammography system (GE Healthcare, Chalfont St Giles, U.K.). Images were acquired at X-ray energies of (A) 25 kV, (B) 35 kV, (C) 45 kV, and (D) 49 kV. Imaging was performed using a rhodium (Rh) anode and Rh filter for images A, B, and C. Image D was obtained using a Rh anode and Cu filter to generate an X-ray spectrum with a mean energy above the I K-edge. Image analysis was performed by placing a circular region of interest (ROI) manually in a uniform region of each sample. The fractional increase in image signal of the dilutions over water was calculated from the mean signal in each ROI.

Cell Cultures. SK-BR-3 breast cancer cells were purchased from American Type Culture Collection (ATCC, Rockville, MD) and were cultured in McCoy's 5A medium in a humidified atmosphere of 5% CO_2 and 95% air at 37 °C. The medium was supplemented with 10% fetal bovine serum, 100 units/mL penicillin, and 100 μg/mL streptomycin. In the absence of a CO_2 tank, a 5% CO_2 environment was supplemented with 24 mM of $NaHCO_3$ and 50 mM of HEPES.

Cell Binding of Nanoparticle Aggregates. Cells were cultured on coverslips in 12 well plates and treated with PAA_{25}-ED-FA stabilized 80/20 $NaGdF_4$:Tb^{3+} NPAs or the equivalent NPAs without folic acid (FA) as a control. Each well was incubated with a NP concentration of 5 mg/mL for various time periods at 37 °C. After this incubation, the cells were washed three times with PBS, fixed with 4% formaldehyde, and placed on the microscope slides. The slide was examined with a Nikon Optiphot 2 Epifluorescence Microscope (Nikon Corporation, Tokyo, Japan) equipped with a 488/520 nm excitation/emission filter combination.

Cellular Uptake of Nanoparticles. Cellular uptake of the nanoparticle aggregates was studied using an Olympus FluoView 300 confocal scanning laser microscope. A PlanApo NA 1.40 60X oil-immersion objective was used for excitation and fluorescence collection through a 150 μm confocal pinhole. The excitation source was a 488-nm Ar-ion laser (Melles Griot) operated at an effective power of 160 μW. SK-BR-3 cells were cultured in Willco wells (Catalog No. GWSt-5040) and treated with PAA_{25}-ED-FA stabilized 80/20 ($NaGdF_4$:Tb^{3+}) NPAs or the equivalent NPAs without folic acid (FA) at 6 mg/mL for 2 or 12 h at 37 °C. After the incubation, the cells were washed three times with PBS. The wells were then studied immediately at room temperature. Confocal fluorescence image sections of the culture were acquired at 500-nm intervals and processed using the FluoView software (version Version 4.3, Olympus Canada). Pseudocoloring was applied post-acquisition—Channel 1 (505−575 nm): green, Channel 2 (575 nm or longer): orange—resulting in the NPAs appearing yellow. After the confocal sections were obtained, bright-field transmission images were also acquired to further identify the origin of the fluorescence.

Electron Microscopy. Nanoparticle aggregates were examined with a Hitachi Model H-7000 scanning transmission electron microscopy (STEM) system operating at

(63) Dong, C. H.; Van Veggel, F. C. J. M. *ACS Nano* **2009**, *3*, 123–130.

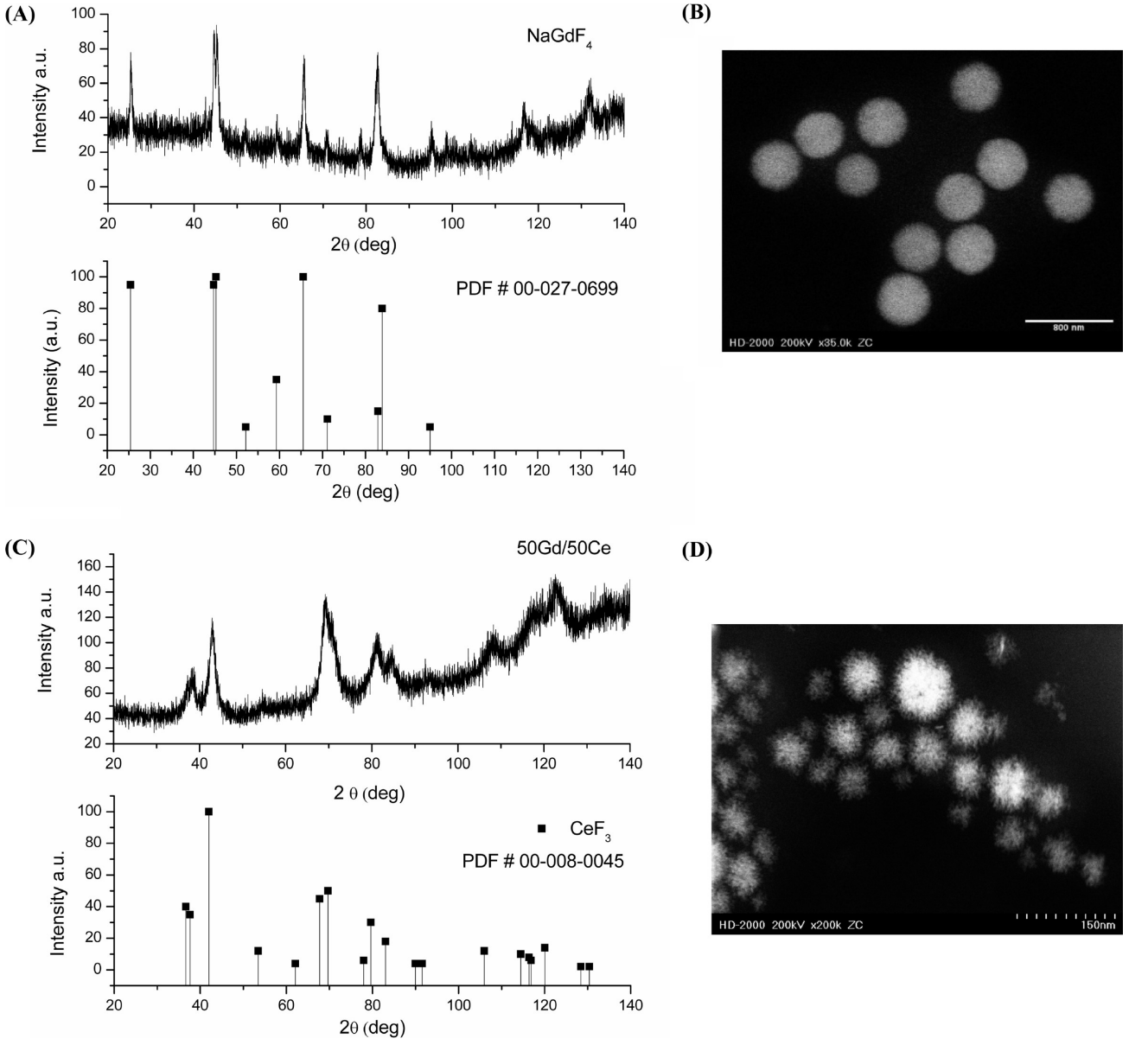

Figure 1. (A) X-ray diffraction (XRD) analysis of powder samples from citrate-stabilized $NaGdF_4$ NPAs. (B) Scanning transmission electron microscopy (STEM) image of PAA_{25}-stabilized GdF_3 NPAs. (C) XRD of PAA_{25}-stabilized GdF_3/CeF_3 NPAs; the lanthanide components are present as a statistical mixture in equal stoichiometric ratios. (D) STEM image of PAA_{25}-stabilized 50/50 GdF_3/CeF_3 NPAs.

an accelerating voltage of 200 kV. The grids were prepared by coating 200 mesh copper grids (Sigma−Aldrich) with a solution of 0.5% Formvar in 1,2-ethylene dichloride. A drop of the lanthanide nanoparticle aggregate solution (~10 mg/mL) was placed on the grid for 1 min, and then it was drawn off by capillary action, using a Kimwipe. Dark-field images were then acquired.

Dynamic Light Scattering. Right-angle dynamic light scattering (DLS) measurements were performed with a commercial laser light scattering spectrometer (ALV/DLS/SLS-5000) that was equipped with an ALV-5000/EPP multiple digital time correlator and laser goniometry system (ALV/CGS-8F S/N 025) with a He-Ne laser (Uniphase 1145P, output power of 22 mW and wavelength of 632.8 nm) as the light source.

Zeta Potential Measurements. Zeta potential (ζ) measurements (data not shown) were conducted using a Zetasizer 3000HS (Malvern Instruments, Worcestershire, U.K.), to confirm the dispersibility and sample stability. The instrument was flushed with 15 mL of deionized water before 5 mL of diluted nanoparticle aggregate solution was injected into it. Five replicates were taken for each nanoparticle aggregate sample, the average of which was reported as the ζ value.

Results and Discussion

I. Synthesis and Characterization. The coprecipitation method, which has been described in detail in the Materials and Methods section, is designed to produce aqueous dispersions of polymer-stabilized $NaGdF_4$ or LnF_3 NPAs. The latter NPAs consist of a 50/50 mixture of GdF_3 and CeF_3, and are coated by linear poly(acrylic acid) polymers (PAA_{25}). In cases where cell imaging was

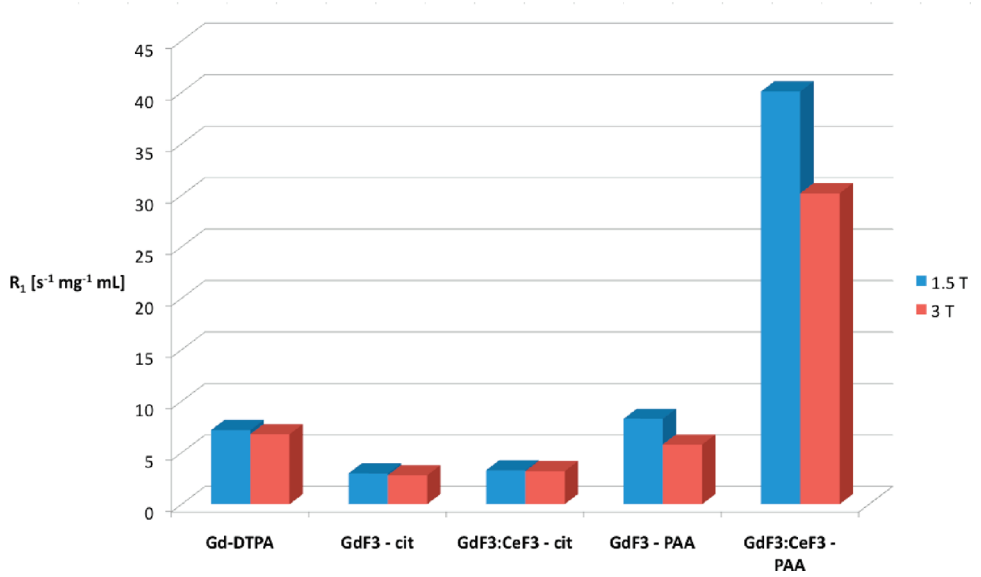

Figure 2. Comparison of mass relaxivities obtained from aqueous dispersions of Gd^{3+}-DTPA, citrate-stabilized $NaGdF_4$ NPAs, citrate-stabilized 50/50 GdF_3/CeF_3 NPAs, and PAA_{25}-stabilized $NaGdF_4$ NPAs or PAA_{25}-stabilized 50/50 GdF_3/CeF_3 NPAs. Relaxivities are provided for both 1.5 T (blue) and 3.0 T (red).

desired, a third formulation was used, consisting of an 80/20 mixture of Gd^{3+} and Tb^{3+} (i.e., $NaGdF_4$:Tb^{3+}). A second batch of PAA_{25}-stabilized NPAs was prepared, wherein the PAA_{25} was covalently coupled to folic acid (FA) via an ethylene diamine (ED) linker. Briefly, an aqueous lanthanide nitrate salt solution was first added dropwise to a solution of citric acid and sodium fluoride at 75 °C under controlled stirring conditions. An aqueous solution consisting of PAA_{25} or (PAA_{25}-ED-FA) in 5 mL of distilled water was then pipetted into the citrate NPA dispersion, to allow for exchange over a period of 12 h. The nanoparticle aggregates were first cooled to room temperature and then precipitated in ethanol, followed by two rounds of resuspension and subsequent precipitation with acetone. An extensive series of reaction conditions was explored with the goal of producing monodisperse NPAs with high relaxivities (see Cheung et al.[64]). The most-sensitive parameters proved to be the stir rate and the cerium dopant levels.

The precipitation method with Gd^{3+} ions only resulted in $NaGdF_4$ particles, as confirmed by XRD measurements. The measured peaks match those of a hexagonal form of $NaGdF_4$. Using Scherrer's equation, the NP diameters are estimated from the XRD profile to be 20−22 nm (Figure 1A). Energy-dispersive X-ray spectroscopy (EDS) confirmed the presence of F, Na, and Gd (see Figure S1F in the Supporting Information). However, the STEM picture (Figure 1B) shows an average diameter of 400 nm. Magnification of the images showed that these nanoparticle aggregates consist of many smaller inorganic nanoparticles with similar sizes to those obtained by XRD (see Figure S1A in the Supporting Information). Note that the STEM images of the NPAs appear the same whether PAA_{25} or citrate is used as a stabilizer, as shown by Figures S1B and S1C in the Supporting Information.

(64) Cheung, E. V. N. et al. Manuscript in preparation.

When Ce^{3+} ions were combined with Gd^{3+} ions in the reaction mixture, nanoparticles consisting of a mixture of CeF_3 and GdF_3 were formed (see Figure S1D in the Supporting Information). The XRD peaks shown in Figure 1C can be matched with the hexagonal phase of CeF_3. The peaks are broader than in the case of $NaGdF_4$, which shows that the NPAs consist of nanoparticle units that are 10−12 nm in diameter. EDS confirmed the presence of F, Na, Gd, and Ce (see Figure S1F in the Supporting Information). The ratio of Ce to Gd was 1.3 ± 0.1. The STEM images (Figure 1D) show NPAs whose diameters are 70 nm. The overall distribution of nanoparticle aggregate sizes can be seen in the STEM images. The average hydrodynamic diameter and polydispersity of the NPAs was determined to be 108 nm and 0.21, respectively, as measured by dynamic light scattering (DLS), shown in Figure S1E in the Supporting Information. Note that the peaks in the XRD of the GdF_3/CeF_3 sample have shifted, relative to those of pure CeF_3, because of the doping of Gd^{3+} ions, which reflects the shrinkage of the unit cell. This is because Ce^{3+} ions are larger than Gd^{3+} ions.[65] Interestingly, the triclinic lattice structure, which is characteristic of CeF_3, is favored in this mixture, as was observed for LaF_3 doped with Gd^{3+}.[65]

II. MRI Relaxivity Measurements. As noted above, the addition of Ce^{3+} helped to significantly lower the average NPA size from 400 nm to 70 nm, which corresponds to an increase in the overall LnF_3 surface area to volume ratio by a factor of 5.7. At nominal doping levels of 50%, the relative surface concentration of Gd^{3+} in the GdF_3/CeF_3 NPAs is thus expected to be ~3 times that of the pure $NaGdF_4$ NPAs, assuming that Gd^{3+} and Ce^{3+} are homogeneously distributed. Since paramagnetic relaxation

(65) Dong, C.; Raudsepp, M.; van Veggel, F. C. J. M. *J. Phys. Chem. C* **2009**, *113*, 472–478.

effects arise primarily from the Gd^{3+} surface concentration, we would therefore expect the ratio of relaxivities of the 50/50 GdF_3/CeF_3 NPAs to those of the $NaGdF_4$ NPAs to be ~3. Figure 2 reveals that, in the case of PAA_{25}-stabilized NPAs, this relaxivity ratio is closer to 6 times, for which there are several possible explanations:

(1) The hexagonal lattice structure associated with the presence of Ce^{3+} results in a more favorable surface, from the perspective of paramagnetic relaxation and interactions between water and Gd^{3+}.[66] The hexagonal structure may also affect the geometry of the Gd^{3+}−water interactions and the exchange time, τ_{ex}.

(2) There could be a slight excess of Gd^{3+} on the surface.

(3) The T_{1e} value of the GdF_3/CeF_3 NPAs may be greater than that in the pure $NaGdF_4$ NPAs, which would also improve relaxivities at the MRI field strengths considered.

(4) The GdF_3/CeF_3 NPAs may possess more-convoluted surfaces, leading to greater interactions with water and higher relaxivities.

Figure 2 also compares relaxivities between aqueous dispersions of NPAs (from a single synthesis batch) that have been stabilized in either citrate or PAA_{25}. The citrate-stabilized NPAs exhibit surprisingly low relaxivities. ^1H NMR magnetization exchange experiments of citrate-coated YF_3 NPAs reveal that the citrate species exchange with the NP surfaces on a time scale of ≤1 s (Alvares et al.[67]). The citrate-stabilized LnF_3 NPAs are also considerably less colloidally stable in solution than their PAA_{25}-stabilized counterparts. Poly(acrylic acid) dramatically enhances the relaxivities by more than a factor of 2 in the case of the $NaGdF_4$ NPAs and by more than an order of magnitude in the case of the smaller GdF_3/CeF_3 NPAs. These relaxivities, which are comparable at both 1.5 and 3.0 T, are considerably higher (i.e., 6−8 times) than those of the clinical standard, Gd^{3+}-DTPA. At present, we can only speculate as to why poly(acrylic acid) gives rise to such an improvement in relaxivity over citrate as the coating agent. It is possible that PAA_{25} allows better coverage of water molecules on the NPA surface (i.e., higher P_m) and/or that it influences water exchange rates (k_{ex}). Note from the ζ potential measurements, shown in Table 1, that both citrate- and PAA_{25}-stabilized NPAs impart high negative surface charge to the NPAs. Surprisingly, the ζ potentials are lower in the case where PAA_{25} is used as a stabilizer, rather than citrate, despite the fact that the PAA_{25}-stabilized NPAs are less prone to precipitation and aggregation over time. Presumably, PAA_{25} is not confined to a thin layer but is diffusely associated with the nanocrystal surface, giving rise to a lower ζ potential. Ideally, the polymer will not prohibit close contact between water and the paramagnetic surface, while sterically perturbing the water−Gd^{3+} interactions to the point where the water exchange rates are optimal for relaxivity.

Table 1. Zeta Potential (ζ) Measurements of Citrate-, PAA_{25}-, and PAA_{25}-ED-FA-Stabilized Lanthanide Trifluoride Nanoparticle Aggregates[a]

nanoparticle aggregate composition	ζ (mV)	sd[a]
citrate-stabilized $NaGdF_4$	−72.6	0.1
PAA_{25}-stabilized $NaGdF_4$	−37.0	0.4
citrate-stabilized GdF_3:CeF_3	−41.1	0.2
PAA_{25}-stabilized 50/50 GdF_3/CeF_3	−17.2	6.5
FA-ED-PAA_{25}-stabilized 80/20 $NaGdF_4$:Tb^{3+}	−73.9	4.3

[a] Standard deviations were obtained from the average of five measurements.

Finally, depending on the surface structure of PAA_{25}, the second hydration sphere of water molecules may be coordinated by PAA_{25} and may play a greater role in contributing to the overall relaxation. In any case, the relaxivity features of the PAA_{25}-stabilized GdF_3/CeF_3 NPAs make them an ideal candidate for MRI imaging, particularly in applications such as perfusion imaging or imaging of very small tumors, where the local concentration of the contrast agent may be limiting. Many papers in the literature quote molar relaxivities (i.e., relaxation rates per Gd^{3+}) while disregarding the mass of the entire complex. In many cases, the matrix is so overwhelmingly large that the effective Gd^{3+} concentration that is achievable is very small and, thus, the potential gains over Gd^{3+}-DTPA or Gd^{3+}-DOTA are not substantial. In contrast, the above polymer-stabilized NPAs are readily soluble at a concentration of 250 mg/mL and possess a high mass fraction of Gd^{3+}, meaning that very high relaxivities are attainable, even after intravenous administration and subsequent dilution. The relaxivity measurements reported in this paper take into account the mass of the core and polymer stabilizers.

III. Fluorescence and Confocal Microscopy Studies of Cellular Uptake and Binding by Folate-Functionalized Polymer-Stabilized $NaGdF_4$:Tb^{3+} NPAs. One clear advantage of the polymer-stabilized nanoparticle aggregates over small molecule contrast agents is the ease with which they can be functionalized and thus targeted. We have experimented with an $\alpha_v\beta_3$-specific cyclized RGDfK peptide[68] and folate[69] as targeting agents, which can be conjugated to PAA_{25} at desired stoichiometries. Poly(acrylic acid) also provides a biological interface that facilitates vascular retention and cell targeting, once functionalized. The lanthanide fluoride NPAs may be visualized by flow cytometry, epi-fluorescence, or confocal microscopy by doping the NPs with Tb^{3+}. While alternative methods of obtaining fluorescence signatures from rare-earth nanomaterials have certainly been demonstrated,[70−73]

(66) Dong, C.; Raudsepp, M.; van Veggel, F. C. J. M. *J. Phys. Chem. C* **2009**, *113*, 472−478.
(67) Alvares, R. D. A. et al. Manuscript in preparation.
(68) Dai, X.; Su, Z.; Liu, J. *Tetrahedron Lett.* **2000**, *41*, 6295–6298.
(69) Rossin, R.; Pan, D.; Qi, K.; Turner, J. L.; Sun, X.; Wooley, K. L.; Welch, M. J. *J. Nucl. Med.* **2005**, *46*, 1210–1218.
(70) Boyer, J. C.; Manseau, M. P.; Murray, J. I.; van Veggel, F. *Langmuir* **2010**, *26*, 1157–1164.
(71) Zhou, J.; Sun, Y.; Du, X. X.; Xiong, L. Q.; Hu, H.; Li, F. Y. *Biomaterials* **2010**, *31*, 3287–3295.
(72) Kumar, R.; Nyk, M.; Ohulchanskyy, T. Y.; Flask, C. A.; Prasad, P. N. *Adv. Funct. Mater.* **2009**, *19*, 853–859.
(73) Gai, S. L.; Yang, P. P.; Li, C. X.; Wang, W. X.; Dai, Y. L.; Niu, N.; Lin, J. *Adv. Funct. Mater.* **2010**, *20*, 1166–1172.

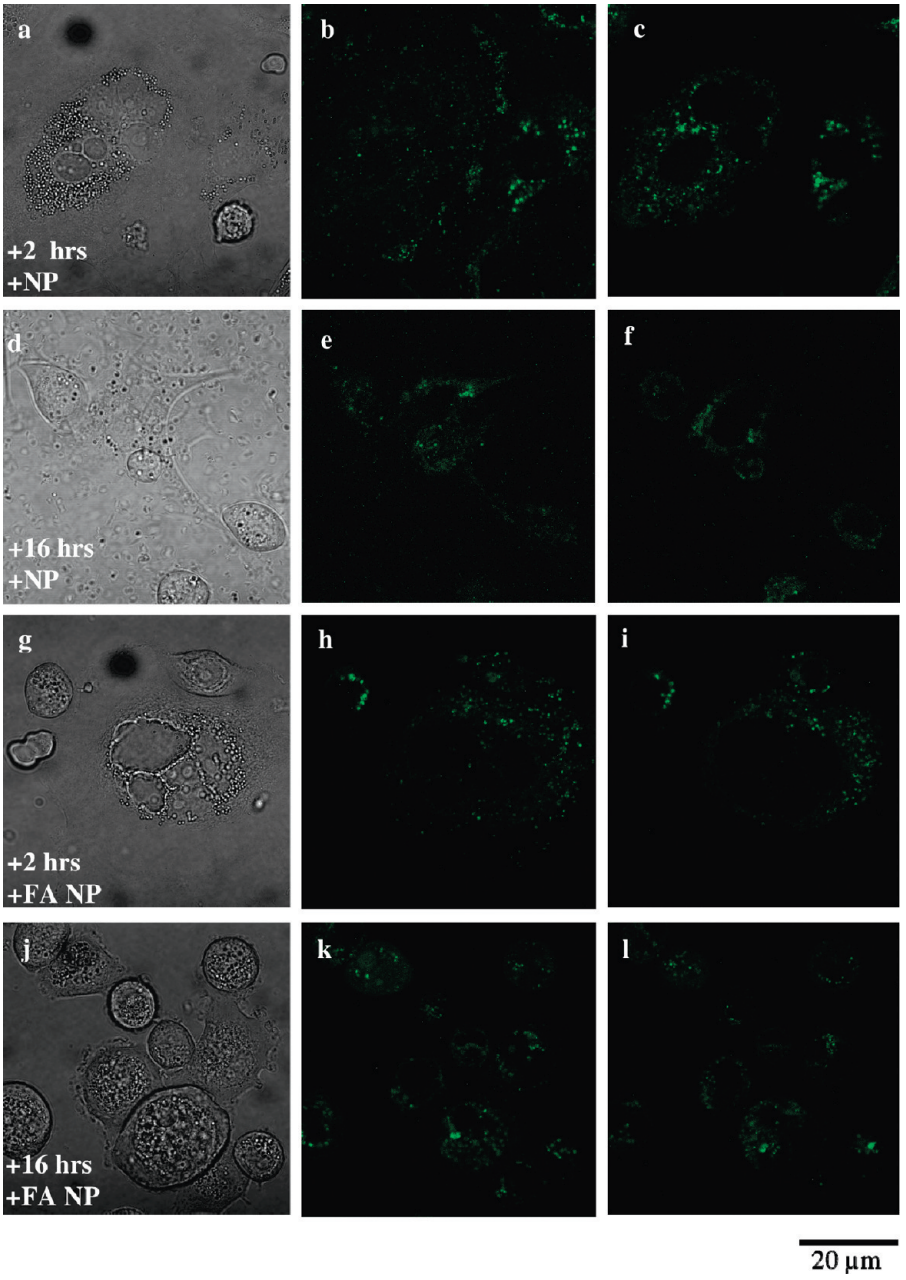

Figure 3. (a, d, g, and j) Light microscopy transmission images and (b, c, e, f, h, i, k, and l) confocal fluorescent images of polymer-stabilized $NaGdF_4$: Tb^{3+} NPAs after incubation with SK-BR-3 cells. Results from cells incubated with folate (+FA)-functionalized NPs (i.e., PAA_{25}-ED-FA stabilized $NaGdF_4$: Tb^{3+} NPAs) are shown in images (g)−(l), whereas those incubated with NPAs without FA are shown in images (a)−(f). Short incubation times result in aggregation of NPAs at the cell periphery, whereas longer incubation times reveal the accumulation of NPs in the cell interior, as shown by confocal microscopy through representative upper slices (third column) and two-dimensional (2D) slices approximately through the cell interior (middle column).

Tb^{3+} ions may also be directly utilized for fluorescence imaging applications.[74−76] Tb^{3+} ions possess very similar excitation and emission wavelength maxima to green fluorescent protein (i.e., 488-nm excitation and 520-nm detection) with the added advantage of narrower absorbance and emission bands, longer lived fluorescence lifetimes, and a lack of photobleaching that aids in eliminating background fluorescence in cell imaging.

In the current study, epi-fluorescence and confocal laser scanning microscopy were used to evaluate the cellular uptake and intracellular distribution of folic acid-functionalized NPAs. SK-BR-3 breast cancer cells, which are known to overexpress folate receptors, were incubated with 6 mg/mL of folate-functionalized NPAs (i.e., PAA_{25}-ED-FA stabilized $NaGdF_4$:Tb^{3+} NPAs). Control studies were also conducted in which SK-BR-3 cells were coincubated with PAA_{25}-stabilized $NaGdF_4$:Tb^{3+} NPAs lacking the folate targeting moieties. Epi-fluorescence microscopy images were first acquired to determine if the NPAs exhibited association with SK-BR-3 cells. Images showed increased fluorescence intensity as a function of

(74) Zhang, C. M.; Li, C. X.; Peng, C.; Chai, R. T.; Huang, S. S.; Yang, D. M.; Cheng, Z. Y.; Lin, J. *Chem.—Eur. J.* **2010**, *16*, 5672–5680.
(75) Kong, D. Y.; Wang, Z. L.; Lin, C. K.; Quan, Z. W.; Li, Y. Y.; Li, C. X.; Lin, J. *Nanotechnology* **2007**, *18*, 1–7.
(76) Li, C. X.; Liu, X. M.; Yang, P. P.; Zhang, C. M.; Lian, H. Z.; Lin, J. *J. Phys. Chem. C* **2008**, *112*, 15602–15602.

incubation time, as shown in Figure S2 in the Supporting Information. Both NP formulations showed good peripheral binding to cells with short incubation periods of 2 h, as shown by Figures 3b and 3c (PAA_{25}-stabilized $NaGdF_4$:Tb^{3+} NPAs) and Figures 3h and 3i (PAA_{25}-ED-FA-stabilized $NaGdF_4$:Tb^{3+} NPAs). Upon longer incubation times (16 h), PAA_{25}-ED-FA-stabilized NPAs were visible within the inner part of the cells (see Figure 3k). Large pockets were also observed within cells, which were likely endosomes formed during receptor-mediated endocytosis, as evidenced by colocalization of endosome-specific antibody stains and confocal microscopy (data not shown). If the wells were left for a period of 2 h or more, we observed that the control sample was endocytosed (to a lesser extent than the PAA_{25}-ED-FA species), because of nonspecific binding. Overall, the folic acid-functionalized NPAs exhibited preferential uptake by SK-BR-3 cells, resulting in increased signal with time.

IV. Animal Perfusion MRI Imaging. Dynamic-contrast-enhanced MRI (DCE-MRI) was performed using 18.6 mg/mL PAA_{25}-stabilized NPAs in a healthy Long Evans rat. Signal enhancement was observed in blood vessels, brain, and muscle, as shown in Figure 4. Contrast was comparable to that of a similar dose of Omniscan (gadodiamide) at 287 mg/mL. The rat was kept under observation for several hours following the injection, and no adverse effects in terms of respiration or pulse were noted during or after administration of either contrast agents. Moreover, phase contrast microscopy revealed obvious changes in red blood cell morphology with equivalent mass concentrations of Omniscan, whereas no detectable changes were observed with equivalent concentrations of the NPAs (see Figure S3 in the Supporting Information).

The extraordinarily high relaxivity of these nanoparticle aggregates will allow for DCE-MRI experiments to be performed at a wide range of relaxivities (corresponding to different concentrations of nanoparticle aggregates), which will help with measurement of physical parameters such as flow, mean transit time, and vascular volume fraction.[77] The large size of these nanoparticle aggregates, relative to Gd^{3+}-DTPA and other small molecule imaging agents, results in slower tissue uptake, which allows for higher resolution imaging, because more time can be spent acquiring each image.

V. Computed Tomography (CT) and Therapeutic Approaches. The PAA_{25}-stabilized NPAs were also evaluated for their potential role as contrast agents for computed tomography (CT). CT is one of the most common diagnostic imaging methodologies and is also suited to the use of Gd^{3+}-based contrast agents at certain X-ray energies. In CT, contrast is achieved through differential attenuation of the incident X-rays. In the diagnostic imaging X-ray energy regime, the dominant attenuation (μ) mechanism is the photoelectric effect that relates to the interaction between the X-rays and the inner shell electrons. This attenuation coefficient tends to be very

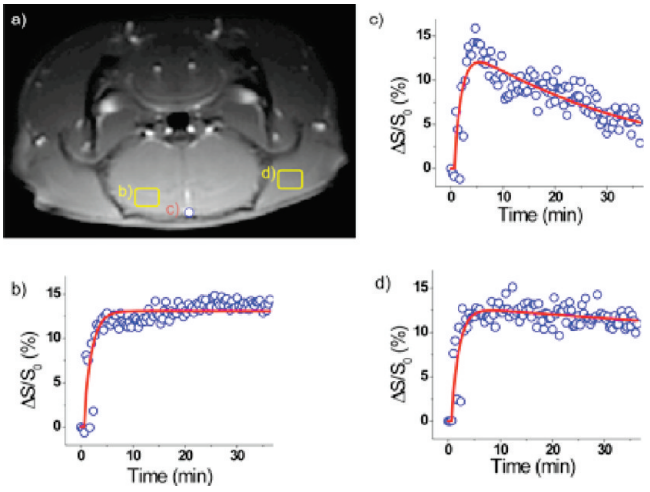

Figure 4. Dynamic contrast enhancement of rat brain following a 0.4 mL injection of 18.6 mg/mL NPA contrast agent. (a) Axial T_1-weighted images were obtained every 20 s following injection for a period of 35 min. Enhancement curves are shown for muscle (denoted by the yellow box marked "b)" in the image), cerebral blood vessel (denoted by area marked "c)" in the image), and brain (denoted by the yellow box marked "d)" in the image). Dynamic contrast enhancement of rat brain following 0.4 mL injection of 18.6 mg/mL nanoparticle contrast agent. Axial T_1-weighted images (a) were obtained every 20 s following injection for a period of 35 min. Enhancement curves are shown for (b) brain (200 voxels), (c) cerebral blood vessel (30 voxels), and (d) muscle (200 voxels). DCE-MRI demonstrates feasibility of using NPAs as perfusion contrast agent at doses 10 times smaller than standard Gd^{3+}-DTPA chelates.

high for low-energy (low-E) incident beams and high-atomic-number (high-Z) absorbers (i.e., $\mu_{\text{photoelectron}} \propto 1/E^3$ and $\mu_{\text{photoelectron}} \propto Z^3$). The choice of the ideal X-ray energy for clinical imaging maximizes contrast between the tissues to be differentiated and minimizes the radiation dose to the patient. Energies such as those found in the middle X-ray range (55−70 keV) are ideal for achieving contrast between bone and soft tissues. Tumor and normal tissues can sometimes be discriminated by X-rays at such energies, but improved contrast can only be achieved with (high-Z) contrast agents designed to selectively partition into one of the two tissues. Iodinated contrast agents are also extraordinary performers as vascular and extravascular contrast agents, because they also exhibit low toxicity and minimal osmotic shock at high dosages.[78] Interestingly, below ~30 keV (the operational regime of conventional mammography) and above 50 keV (the operational regime of conventional CT), the X-ray mass attenuation offered by gadolinium is higher than that achieved by iodine. Gd_2O_3 particulates have been tested as potential CT contrast agents in rabbit abdomens and livers with striking results. Gd^{3+} chelates similar to those used for MRI have also been extensively tested as CT contrast agents.[79,80] Thus, Gd^{3+}-based NPAs may offer real gains in X-ray contrast over current

(77) Shepherd, T. M.; Flint, J. J.; Thelwall, P. E.; Stanisz, G. J.; Mareci, T. H.; Yachnis, A. T.; Blackband, S. J. *Neuroimage* **2009**, *44*, 820–826.
(78) Cademartiri, F.; de Monye, C.; Pugliese, F.; Mollet, N. R.; Runza, G.; van der Lugt, A.; Midiri, M.; de Feyter, P. J.; Lagalla, R.; Krestin, G. P. *Invest. Radiol.* **2006**, *41*, 349–353.
(79) Carrascosa, P.; Merletti, P. G.; Capunay, C.; Goldsmit, A.; Bettinotti, M.; Carrascosa, J. *J. Comput.-Assisted Tomogr.* **2007**, *31*, 441–443.
(80) Alric, C.; Taleb, J.; Le Duc, G.; Mandon, C.; Billotey, C.; Le Meur-Herland, A.; Brochard, T.; Vocanson, F.; Janier, M.; Perriat, P.; Roux, S.; Tillement, O. *J. Am. Chem. Soc.* **2008**, *130*, 5908–5915.

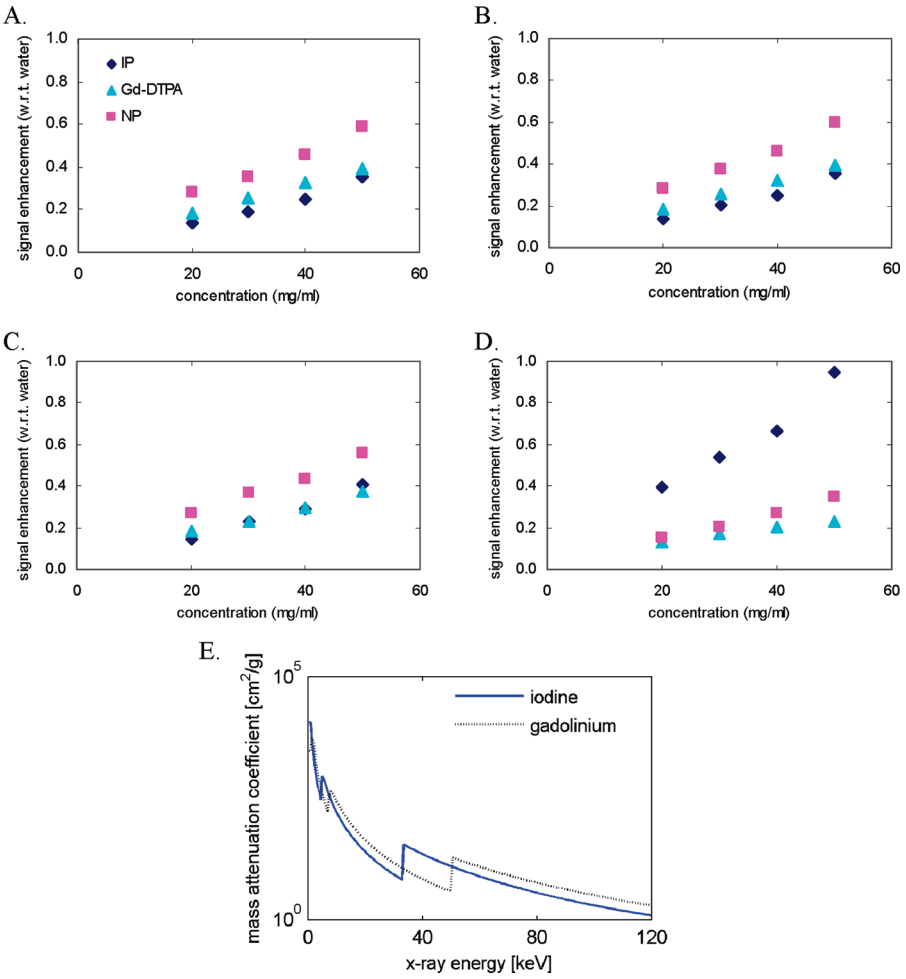

Figure 5. Fractional increase in X-ray image signal as a function of mass concentration of PAA_{25}-coated 90/10 $NaGdF_4:Eu^{3+}$ NPAs, Gd^{3+}-DTPA, and IP (iopromide) samples dilutes in water. Images were acquired on a Senographe 2000D digital mammography system (GE Healthcare, Chalfont St Giles, U.K.) at X-ray energies of (A) 25 kV, (B) 35 kV, (C) 45 kV, and (D) 49 kV. Imaging was performed using a Rh anode and Rh filter for the graphs in panels (A), (B), and (C). The graph shown in panel (D) was obtained using a Rh anode and a Cu filter. Panel (E) shows I and Ga X-ray mass attenuation coefficients, as a function of X-ray energy. The NPAs exhibit an advantage in terms of X-ray attenuation at or above the K-edge of Gd at 50.2 keV and at X-ray energies lower than the K-edge of iodine at 33.2 keV.

iodinated species, assuming it can be demonstrated that toxicity is minimal.

X-ray image signals of samples diluted in water, as a function of mass concentration of PAA_{25}-coated $NaGdF_4:Eu^{3+}$ NPAs, Gd^{3+}-DTPA, and IP (iopromide), are presented in Figure 5, according to the fractional increase in signal over water. Images were obtained at X-rays energies of 25 kV (Figure 5A), 35 kV (Figure 5B), 45 kV (Figure 5C), and 49 kV (Figure 5D), where the associated X-ray spectra mean energies for each image are 17.5 keV, 20 keV, 22 keV, and 38 keV, respectively. Attenuation for Gd^{3+}-based species, relative to that for the iodinated species, is greatest at or above the K-edge of Gd^{3+} (i.e., 50.2 keV) and at X-ray energies lower than the K-edge of iodine (33.2 keV), as shown in Figure 5E. This is consistent with the observation that the X-ray attenuation per unit mass is higher for the Gd^{3+}-based species than the iodinated species at X-ray energies associated with A, B, and C. A closer inspection of Figure 5 also reveals that, at all energies, the Gd^{3+}-based nanoparticle aggregates outperform Gd^{3+}-DTPA at equivalent mass concentrations. The improved behavior of NPAs may arise from a greater surface concentration of counterions or from an effectively larger X-ray absorption cross-section (per unit mass of contrast agent), which has been previously observed with gold- and gadolinium-based NPAs.[80−83] The gold- and Gd^{3+}-based NPAs offer three main advantages over conventional small molecule contrast agents, such as Iopromide: (1) higher X-ray attenuation below 30 keV and above 50 keV, (2) improved vascular retention, and (3) the ability to be functionalized for targeted imaging, whereupon local contrast may be significantly improved.

Recently, the possibility of rendering Gd^{3+}-based nanoparticles as therapeutic agents has been revisited.[51] Gadolinium has the highest thermal neutron capture cross-section of any element and the irradiation of thermal neutrons is known to result in the emission of cytotoxic γ-rays and Auger electrons. Others have discussed the use of

(81) Hainfeld, J. F.; Slatkin, D. N.; Focella, T. M.; Smilowitz, H. M. *Br. J. Radiol.* **2006**, *79*, 248–53.
(82) Kim, D.; Park, S.; Lee, J. H.; Jeong, Y. Y.; Jon, S. *J. Am. Chem. Soc.* **2007**, *129*, 7661–7665.
(83) Huang, M. Q.; Pickup, S.; Nelson, D. S.; Qiao, H.; Xu, H. N.; Li, L. Z.; Zhou, R.; Delikatny, E. J.; Poptani, H.; Glickson, J. D. *NMR Biomed.* **2008**, *21*, 1021–1029.

Gd^{3+} to enhance dose by X-ray irradiation at appropriate energies to release Auger electrons.[84,85] In the latter case, Gd^{3+} should ideally be incorporated in the nucleus of the target cell, since the stopping distances of the X-ray-generated Auger electrons is very short. In either case, the therapeutic applications follow a familiar theme, namely, the ability of the Gd^{3+}-based nanoparticles to be retained in the vasculature and/or functionalized and thus concentrated in or around target cells gives them a significant advantage in terms of the therapeutic index.

Conclusions

We demonstrate the application of a PAA_{25}-stabilized lanthanide fluoride nanoparticle aggregate system consisting of a core of either $NaGdF_4$ or 50/50 CeF_3/GdF_3, for magnetic resonance imaging (MRI) and computed tomography (CT). The two-step synthesis is straightforward and can be tailored to control the size by adjusting the stir rate and combining Ce^{3+} with Gd^{3+}. Very high relaxivities are observed at 1.5 and 3.0 T (i.e. ,mass relaxivities of $35-40\ s^{-1}\ mg^{-1}$ mL, which may be compared to that of Gd^{3+}-DTPA, which is on the order of $7\ s^{-1}\ mg^{-1}$ mL). We attribute these high relaxivities, relative to our earlier GdF_3 NP formulations,[50] to the following: (1) mixing with Ce^{3+}, which gives rise to smaller NPAs and, consequently, higher surface areas and a more favorable crystal structure, and (2) coating with PAA_{25}, which facilitates water interactions with Gd^{3+} on the NP surface while enhancing colloidal stability. We anticipate that the PAA_{25}-stabilized NPAs have other advantages over their small molecule counterparts both in the area of MRI and CT. Their 70−100 nm dimensions should allow for improved retention, particularly in leaky vasculature which characterizes tumors.[86] Moreover, their surfaces can be modified for targeted imaging, as demonstrated by the folate-conjugated $NaGdF_4:Tb^{3+}$ NPAs. Confocal laser scanning microscopy from the Tb^{3+}-doped version of the NPAs confirmed that the folate functionalized NPAs were endocytosed by cancer cells, while preliminary perfusion MRI studies in rats showed no obvious signs of toxicity or rapid accumulation of the NPAs in the lungs or liver. Future studies will focus on targeted imaging applications, where it is anticipated that significant enhancement in signal of small tumors may be realized, because of the preferential partitioning of these NPAs within tumor vasculature and to the preferential ability of cancerous cells to uptake folate-functionalized NPAs.

Abbreviations

Ce^{3+} = cerium ion
CT = computed tomography
DCE MRI = dynamic-contrast-enhanced MRI
DCC = 1,3-dicyclohexylcarbodiimide
DLS = dynamic light scattering
DTPA = diethylenetriaminepentaacetic acid
EDAC = 1-ethyl-3-(3-dimethylaminopropyl)carbodiimide
EDS = energy-dispersive X-ray spectroscopy
Eu^{3+} = europium ion
FA = folic acid
Gd^{3+} = gadolinium ion
IP = iopromide 1-*N*,3-*N*-*bis*(2,3-dihydroxypropyl)-2,4,6-triiodo-5-(2-methoxyacetamido)-1-*N*-methylbenzene-1,3-dicarboxamide
Ln = lanthanide
MES = 2-(*N*-morpholino)ethanesulfonic acid
MRI = magnetic resonance imaging
NHS = *N*-hydroxysuccinimide
NP = nanoparticle
NPA = nanoparticle aggregate
PAA_{25} = linear poly(acrylic acid), consisting of an average of 25 repeating units
PAA_{25}-ED-FA = PAA_{25} coupled to folic acid via an ethylene diamine linker
PBS = phosphate-buffered saline
ROI = region of interest
STEM = scanning transmission electron microscopy
T_1 = longitudinal relaxation time
T_2 = transverse relaxation time
Tb^{3+} = terbium ion
XRD = X-ray diffraction

Acknowledgment. R.S.P. acknowledges NSERC, and the Ontario government, for financial support through the NSERC Discovery (261980) and the Provincial Research Excellence Award (PREA) programs. F.v.V. acknowledges the generous funding from the Natural Science and Engineering Research Council (NSERC), the Canada Foundation for Innovation (CFI), and the British Columbia Knowledge Development Fund (BCKDF) of Canada. C.M.Y. acknowledges support from CIHR Research (Resource Grant No. PRG-80174) and the Canada Research Chairs program. M.L.H. acknowledges NSERC and the support of the Ontario Institute for Cancer Research, through funding provided by the Ontario Ministry of Research and Innovation. We thank the Kumacheva Laboratory at the University of Toronto for assistance in the zeta potential and DLS experiments.

Supporting Information Available: Additional STEM, DLS, and EDS data of NPs and NPAs are provided to give a better impression of size, size distribution, and surface topology. Phase contrast microscopy data assessing cell toxicity in erythrocytes is also included as are light and fluorescence microscopy data of the NPAs. This material is available free of charge via the Internet at http://pubs.acs.org.

(84) Kassis, A. I. *J. Nucl. Med.* **2003**, *44*, 1479–1481.
(85) Aziz, E. F.; Bugaj, J. E.; Caglar, G.; Dinkelborg, L. M.; Lawaczeck, R. *Cancer Biother. Radiopharm.* **2006**, *21*, 181–193.
(86) Storm, G.; Belliot, S. O.; Daemen, T.; Lasic, D. D. *Adv. Drug Delivery Rev.* **1995**, *17*, 31–48.